Synthetic Inhibitors of Bacterial Cell Division Targeting the GTP-Binding Site of FtsZ

ARTICLE *in* ACS CHEMICAL BIOLOGY · JULY 2013

Impact Factor: 5.33 · DOI: 10.1021/cb400208z · Source: PubMed

12 AUTHORS, INCLUDING:

Sonia Huecas
Spanish National Research Council
21 PUBLICATIONS **683** CITATIONS
SEE PROFILE

Marta Artola
Leiden University
5 PUBLICATIONS **32** CITATIONS
SEE PROFILE

Isabel Barasoain
Spanish National Research Council
103 PUBLICATIONS **1,653** CITATIONS
SEE PROFILE

Jose Manuel Andreu
Centro de Investigaciones Biológicas
166 PUBLICATIONS **5,770** CITATIONS
SEE PROFILE

ACS chemical biology

Articles

pubs.acs.org/acschemicalbiology

Synthetic Inhibitors of Bacterial Cell Division Targeting the GTP-Binding Site of FtsZ

Laura B. Ruiz-Avila,[†] Sonia Huecas,[†] Marta Artola,[‡] Albert Vergoñós,[†] Erney Ramírez-Aportela,[†,§] Emilia Cercenado,[∥] Isabel Barasoain,[†] Henar Vázquez-Villa,[‡] Mar Martín-Fontecha,[‡] Pablo Chacón,[§] María L. López-Rodríguez,[‡] and José M. Andreu*[,†]

[†]Centro de Investigaciones Biológicas, CSIC, Madrid, [‡]Dpto. Química Orgánica I, Facultad de Ciencias Químicas, UCM, Madrid, [§]Instituto de Química-Física Rocasolano, CSIC, Madrid, and [∥]Servicio de Microbiología, Hospital General Universitario Gregorio Marañón, Madrid, Spain

Supporting Information

ABSTRACT: Cell division protein FtsZ is the organizer of the cytokinetic Z-ring in most bacteria and a target for new antibiotics. FtsZ assembles with GTP into filaments that hydrolyze the nucleotide at the association interface between monomers and then disassemble. We have replaced FtsZ's GTP with non-nucleotide synthetic inhibitors of bacterial division. We searched for these small molecules among compounds from the literature, from virtual screening (VS), and from our in-house synthetic library (UCM), employing a fluorescence anisotropy primary assay. From these screens we have identified the polyhydroxy aromatic compound UCM05 and its simplified analogue UCM44 that specifically bind to *Bacillus subtilis* FtsZ monomers with micromolar affinities and perturb normal assembly, as examined with light scattering, polymer sedimentation, and negative stain electron microscopy. On the other hand, these ligands induce the cooperative assembly of nucleotide-devoid archaeal FtsZ into distinct well-ordered polymers, different from GTP-induced filaments. These FtsZ inhibitors impair localization of FtsZ into the Z-ring and inhibit bacterial cell division. The chlorinated analogue UCM53 inhibits the growth of clinical isolates of antibiotic-resistant *Staphylococcus aureus* and *Enterococcus faecalis*. We suggest that these interfacial inhibitors recapitulate binding and some assembly-inducing effects of GTP but impair the correct structural dynamics of FtsZ filaments and thus inhibit bacterial division, possibly by binding to a small fraction of the FtsZ molecules in a bacterial cell, which opens a new approach to FtsZ-based antibacterial drug discovery.

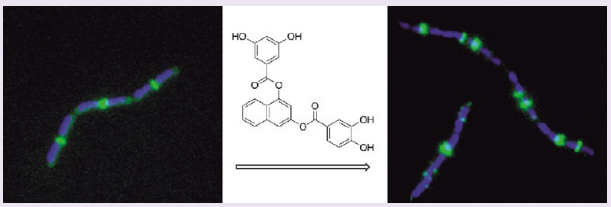

FtsZ is the key protein for division of most bacterial cells and an attractive antibacterial target. It forms the Z-ring, which marks the division site and recruits the other divisomal proteins.[1,2] FtsZ is a self-assembling GTPase that shares the structural fold of eukaryotic tubulin.[3] It assembles into polar tubulin-like protofilaments in which the GTP-binding site of one monomer is at the association interface with the next monomer completing the GTPase site.[4−6] Dynamic FtsZ filaments bend and depolymerize upon GTP hydrolysis, and laterally associate in different fashions including double filaments, bundles, and ribbons.[7,8] The Z-ring structure has been visualized by electron cryotomography as an array of relatively short FtsZ filaments, encircling the cell below the plasma membrane.[9] The constriction of the Z-ring during cell division is thought to work by a combination of FtsZ filament condensation, sliding, bending, and recycling events.[7]

New antibiotics are clearly needed to fight the widespread emergence of bacterial pathogens resistant to current therapeutic options.[10−12] FtsZ-related approaches to antibiotic discovery have included high-throughput screens with *in vitro*[13] or cell-based assays,[14,15] screening for inhibitors of binding of FtsZ by its divisomal partner ZipA,[16] enhancing FtsZ degradation by activating protease ClpP with acyldepsipeptide antibiotics,[17] and antisense RNA-peptide conjugates targeting the *ftsZ* gene.[18] Focusing on site-directed approaches, the main cavities available for ligand binding in a FtsZ monomer are the nucleotide-binding cup and the long cleft between its GTP-binding and C-terminal domains.[19] A growing number of small molecules have been reported to interact with FtsZ and bacterial cell division [reviewed in refs 20−23], although the specificity and binding site on FtsZ have only been established in a few cases.

The difluoro-benzamide derivative PC190723 effectively inhibits bacterial cell division, protected mice from a lethal dose of *S. aureus* (Sa), and served to validate FtsZ as an antibacterial target.[24] This compound has been reported to restore methicillin-resistant *S. aureus* susceptibility to β-lactam antibiotics[25] and has recently been optimized into a more potent drug candidate.[26] PC190723 and its closely related analogue 8j impair the correct assembly of the Z-ring, delocalizing FtsZ into multiple foci throughout *Bacillus subtilis* (Bs) cells.[24,27] We found that PC190723 binding does not

Received: March 27, 2013
Accepted: July 15, 2013
Published: July 15, 2013

inhibit but induces the assembly of Bs-FtsZ and Sa-FtsZ protofilaments and condensates,[28] possibly by drugging the FtsZ assembly switch,[29] which may explain the disorganization of the Z-ring in bacterial cells. Recently, the new structures of FtsZ from Sa-FtsZ[5,6,25] have shown the C-terminal domain rotated into an open conformation, different from the closed conformation of all the other FtsZ structures. This Sa-FtsZ open conformation (i) allows the binding of PC190723 into the cleft between the two domains of FtsZ, explaining the modulation of FtsZ assembly by this ligand; (ii) facilitates the formation of a tight binding interface between FtsZ monomers in a continuous straight protofilament in the crystals, burying the nucleotide in contrast with its accessibility in the archaeal FtsZ dimer;[4] and (iii) reveals the possible structural mechanism of the FtsZ assembly switch. To confirm this mechanism, both the closed and the open FtsZ structures should be observed with the same protein, i.e., obtaining a closed Sa-FtsZ structure or an open structure from other FtsZ.

Focusing on the GTP-binding site of FtsZ, we employed fluorescent *mant*-GTP as a probe to determine the energetics and kinetics of nucleotide binding to model FtsZ from the thermophilic archaea *Methanococcus jannaschii* (Mj-FtsZ), in its monomer and polymer forms.[30] On the other hand, the modified nucleotide C8 Br-GTP had been shown to inhibit polymerization of Ec-FtsZ.[31] This was followed by a series of C8-substituted GTP analogues that inhibit FtsZ polymerization while supporting tubulin assembly, revealing differences between their nucleotide-binding sites,[32] which constituted a proof of concept for targeting FtsZ with selective inhibitors that would not poison eukaryotic tubulin. However, these charged GTP analogues lacked antibacterial activity, possibly because they do not pass the bacterial envelope, and the prodrug strategies explored were unsuccessful.[33] Therefore, we took the challenge of finding non-nucleotide inhibitors that could enter bacterial cells and replace GTP at the FtsZ nucleotide site. To these purposes we developed a *mant*-GTP fluorescence anisotropy competitive assay to measure the binding of any molecule to the nucleotide-binding site of archaeal Mj-FtsZ.[34]

In this work we have searched for small molecules targeting the nucleotide-binding site of FtsZ using multiple strategies. Here we describe non-nucleotide synthetic molecules that effectively compete with GTP for binding to FtsZ and analyze their mechanism of action on Bs-, Ec-, and Mj-FtsZ proteins. We also report the impairment of the division Z-ring by these compounds and their antibacterial activities, aiming at FtsZ's GTP-replacing antibiotics.

RESULTS AND DISCUSSION

Non-nucleotide Ligands Replacing GTP in FtsZ. To search for small molecules that could replace the nucleotide in FtsZ, we conducted three selective screens: compounds from the literature, virtual screening (VS) hits, and in-house compounds. We employed the *mant*-GTP anisotropy method[34] adapted to bacterial Bs-FtsZ (Methods) as a primary assay in our quest.

Compounds from the Literature. We tested several available compounds among those reported to interact with FtsZ.[23] Totarol, the heterocyclic compound sanguinarine, and cinnamaldehyde had given negative results before with Mj-FtsZ.[34] In this work, amikacin and the polyphenolic compounds curcumin, caffeic acid, and chlorogenic acid gave also negative results, despite of their good predictive docking scores into the GTP-binding site of Bs-FtsZ.[23] Moreover, we were interested by the bacterial division inhibitors PC58538 and PC170942, since resistance mutations map around the GTP-binding site.[14] We synthesized the more active PC170942 (Methods) but found that it did not displace *mant*-GTP from Bs-FtsZ within its solubility limit (Supplementary Figure S1). However, PC170942 (15−20 μM) effectively inhibited Bs-FtsZ assembly and *B. subtilis* cell division, but inhibition of GTPase activity was observed at higher concentrations (Supplementary Figure S1). We thus confirmed that PC170942 is a functional inhibitor of FtsZ, but it either competes with GTP too weakly, inhibits assembly by binding to another site at the polymerization interface, or binds to an allosteric site. PC170942 has been recently classified by others as likely forming aggregates.[35] Note, however, that in order to rule out formation of aggregates causing nonspecific inhibition effects,[36,37] we tested the solubility of all the molecules under study in the assay buffer by ultracentrifugation and spectrophotometric measurements (Methods). Such large aggregates can also be easily detected during the *mant*-GTP fluorescence anisotropy measurements, because they would scatter highly polarized light,[38] interfering with the measurements. We also checked each compound for any interference with *mant*-GTP fluorescence and for direct interaction with this probe. In summary, we had tested 8 compounds from the literature without finding an effective inhibitor of GTP binding to FtsZ.

Virtual Screening. We conducted a VS campaign, employing the nucleotide-binding site from the crystal structure of Bs-FtsZ and the ICM docking algorithm.[39] Previous VS with a different approach was unsuccessful.[34] We now screened ~4 × 10^6 compounds, from which we acquired 42 better scoring molecules (Supporting Information). One of them, compound VS2.18 (**1**, Figure 1), competes with *mant*-GTP for binding to Bs-FtsZ with an apparent affinity K_b = (1.1 ± 0.4) × 10^4 M^{-1}. However, VS2.18 lacks antibacterial activity on *B subtilis* (MIC > 600 μM).

In-House Compounds. We simultaneously tested 18 synthetic compounds selected from our in-house library after docking into the Bs-FtsZ GTP site, finding several polyhydroxy derivatives that competitively displace *mant*-GTP from Bs-FtsZ (Figure 1). Compound UCM05 (**2**)[40] has a K_b = (4.30 ± 0.04) × 10^5 M^{-1}. Its fragments UCM16 (**3**) and UCM17 (**4**) retain significant affinity, K_b = (3.0 ± 0.9) × 10^4 M^{-1} and (3.9 ± 1.3) × 10^4 M^{-1}, respectively, with a similar ligand efficiency.[41] We then synthesized a series of analogues and observed that the simplified tetra-hydroxy analogue UCM44 (**5**) has affinity 3.5 times larger than that of UCM05, K_b = (1.5 ± 0.3) × 10^6 M^{-1}, similar to that of the chlorinated analogue UCM53 (**6**) (K_b = (1.3 ± 0.2) × 10^6 M^{-1}), but still ~20-fold lower than the affinity of GTP (K_b = (3.1 ± 0.5) × 10^7 M^{-1}). The binding of UCM05 and UCM44 (20 μM) to Bs-FtsZ (0.5 μM) is relatively slow, $t_{1/2app}$ ≈ 80 s monitored by the *mant*-GTP anisotropy decay. We confirmed that UCM05 and UCM44 replace the nucleotide in Bs-FtsZ and Mj-FtsZ employing a secondary assay that measures the binding of isotopically labeled ^{3}H-GTP (no added fluorescent group) following high-speed centrifugation,[34] from which we obtained compatible K_b values (Figure 2).

We observed that these GTP-replacing small molecules inhibit the growth of the Gram-positive bacterium *B. subtilis* (MIC values: UCM05, 100 μM; UCM44, 25 μM; UCM53, 13 μM) but lack activity on the Gram-negative bacterium *E. coli*. Compound UCM05 has been previously described as a synthetic inhibitor of fatty acid synthase (FASN) with

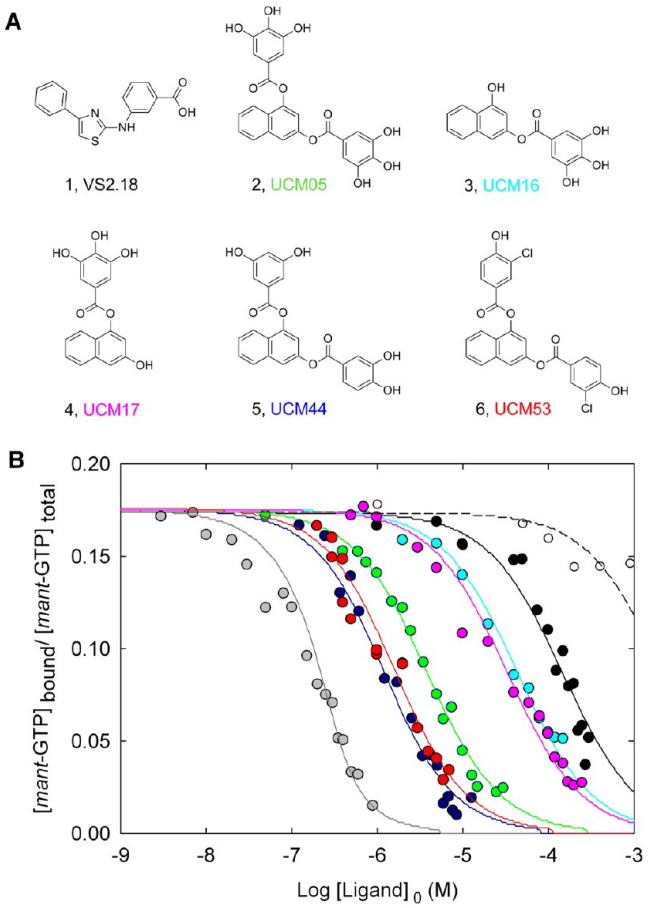

Figure 1. (A) Small molecules competing with nucleotide for binding to FtsZ. (B) Displacement curves of *mant*-GTP (500 nM) from Bs-FtsZ (300 nM binding sites) by the competing ligands, measured by fluorescence anisotropy. The solid lines are best fits to the data, according to a single site competition model. Gray dots, GTP control (K_b = 3.1 × 10^7 M^{-1}). Open black circles, amikacyn, an example of negative result ($K_b \leq 10^3$ M^{-1}; the dashed line is a theoretical curve for K_b = 10^3 M^{-1}). Solid black dots and line, compound VS2.18 (1). Green, compound UCM05 (1). Cyan, fragment UCM16 (3). Pink, fragment UCM17 (4). Dark blue, analogue UCM44 (5). Red, analogue UCM53 (6).

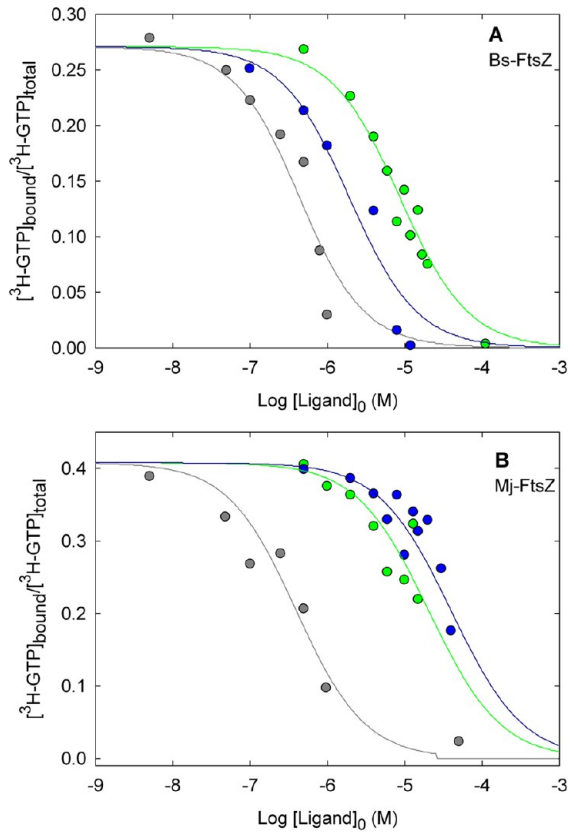

Figure 2. (A) Displacement of ^{3}H-GTP (100 nM) from Bs-FtsZ (60 nM binding sites) by UCM05 (green dots), UCM44 (blue dots), and GTP (gray dots). The lines correspond to best fitted K_b values of the competitors: UCM05, 2.3 × 10^5 M^{-1}; UCM44, 1.1 × 10^6 M^{-1}; GTP, 5.1 × 10^6 M^{-1} (see Methods). (B) A similar experiment with Mj-FtsZ. The best fitted K_b values are UCM05, ∼1.9 × 10^5 M^{-1}; UCM44, ∼1.0 × 10^5 M^{-1}; GTP, 1.1 × 10^7 M^{-1}.

anticancer activity[40,42] related to (−)-epigallocatechin-3-gallate (EGCG). EGCG binds weakly to Bs-FtsZ (K_b = (8.9 ± 2.5) × 10^3 M^{-1}), and the small fragments of UCM05 gallic acid (200 μM) and dihydroxynaphtalene (400 μM) did not compete with *mant*-GTP for binding to Bs-FtsZ. These three compounds lacked antibacterial activity in our tests. The structure−activity relationships in a complete series of UCM05 analogues will be reported elsewhere. In this study we focus on the mechanisms of action of UCM05 and UCM44 on FtsZ and their effects on bacterial cell division together with the less soluble derivative UCM53.

Interactions of Bacterial FtsZ Monomers and Dimers with UCM05 and UCM44. We sought direct evidence of the binding of UCM05 and UCM44 to FtsZ and asked whether guanine nucleotide would displace the ligands binding. The interaction of UCM05 with Bs-FtsZ was examined by differential absorption spectroscopy. The protein modifies the UV absorption bands of the ligand at 286 and 336 nm, and this effect is abolished by GTP addition (Supplementary Figure S2). The protein-induced difference spectrum around 336 nm resembles a pH 6.8 vs pH 7.5 difference spectrum of the ligand alone, suggesting that Bs-FtsZ preferentially binds the protonated form rather than a phenolate anion of UCM05.

The binding of UCM05 and UCM44 to Bs-FtsZ was monitored by simultaneously measuring the sedimentation velocity of the protein and ligands in analytical ultracentrifugation (AUC) experiments (Figure 3). The protein was measured by refractive index increment, and the ligand was monitored by light absorption at 315 nm, where the protein does not interfere. Bs-FtsZ alone sedimented predominantly as $s_{20,w}$ = 2.7 S monomers.[43] UCM05 enhanced the formation of Bs-FtsZ dimers with $s_{20,w}$ = 4.0 S and formed a co-sedimenting boundary at 4.0 S. UCM05 co-sedimentation and FtsZ dimerization were both suppressed by GDP. The ligand did not sediment in the absence of FtsZ, confirming lack of aggregation of the compound. Similar results were obtained with UCM44 (Supplementary Figure S3). We observed, however, that high ligand concentrations (>40 μM UCM05 with 20 μM Bs-FtsZ) induced further self-association of the protein that sedimented to the bottom of the cell. This process was also inhibited by GDP, which suggests a specific ligand-induced association rather than nonspecific protein aggregation.

Modulation of Bacterial FtsZ Assemblies by UCM05 and UCM44. Although the GTP-binding site is well conserved among FtsZ monomers from different species,[44] in the distinct bacterial Sa-FtsZ filament structure the nucleotide gets buried

dx.doi.org/10.1021/cb400208z | *ACS Chem. Biol.* 2013, 8, 2072−2083

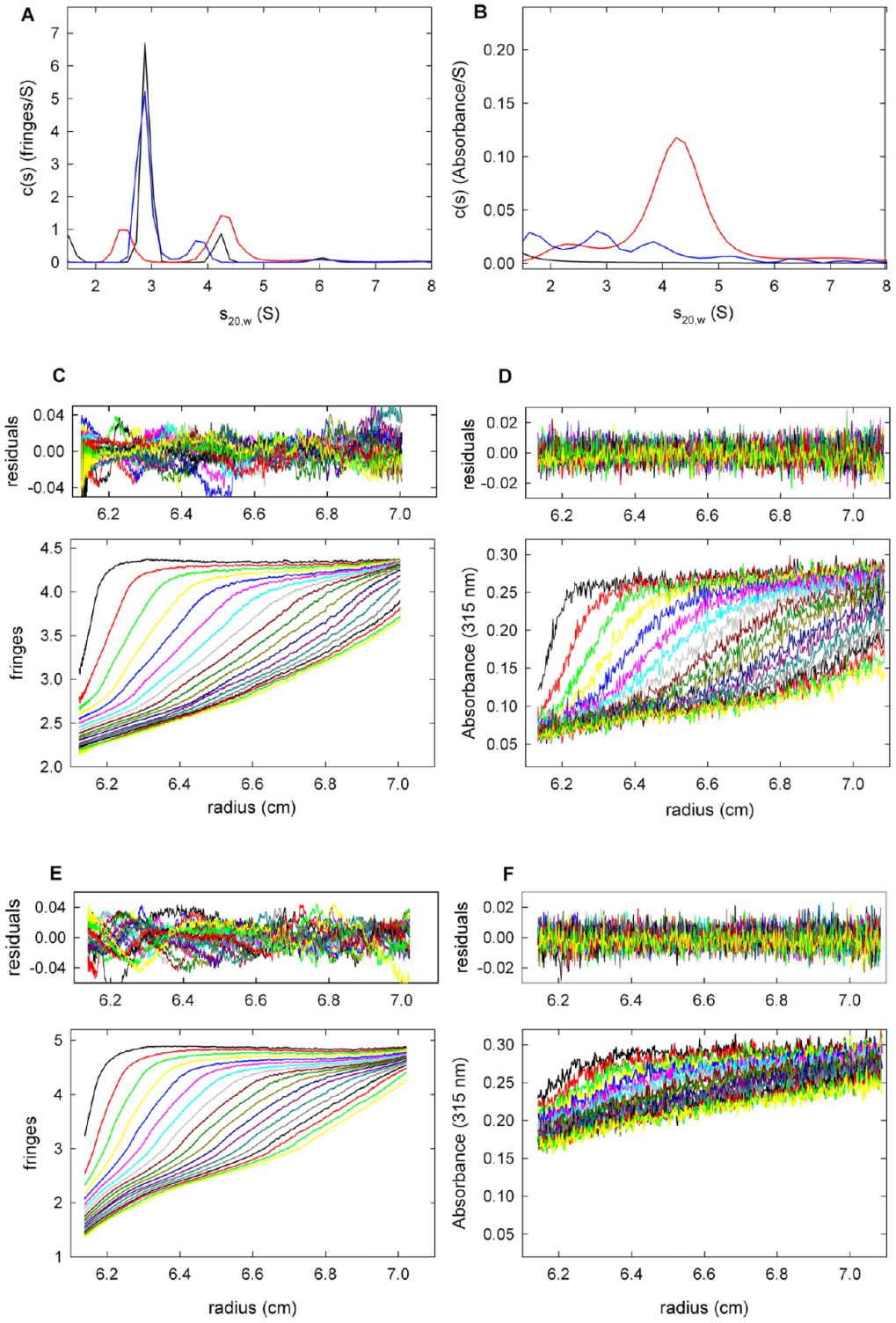

Figure 3. Binding of UCM05 to Bs-FtsZ analyzed with sedimentation velocity AUC. (A) Sedimentation coefficient distribution c(s) of 20 μM FtsZ with 100 μM GDP (black line, main peak average $s_{20,w}$ = 2.7 S), with 40 μM UCM05 (red, 2.3 and 4.0 S) and with UCM05 plus 200 μM GDP (blue, 2.7 S). (B) Corresponding sedimentation coefficient distributions of 40 μM UCM05 alone (black), with 20 μM FtsZ (red, 4.0 S) and with FtsZ plus GDP (blue). From the area under the main ligand and protein peaks, it was calculated that ~1.6 UCM05 molecules co-sedimented per each FtsZ molecule. This number is greater than 1 due to inaccuracy of the method and possibly to nonspecific binding. In a similar experiment made with 20 μM UCM44, ~1.0 ligand molecules co-sedimented per each FtsZ molecule (Supplementary Figure S3). The following panels show AUC data from which the distributions in panels A and B were obtained (Methods). The residuals of the fits are also shown. (C) Successive radial interference scans showing the distribution of FtsZ (20 μM) in the presence of UCM05 (40 μM) during sedimentation. Only one from each two scans is shown. (D) Corresponding radial absorbance scans showing the co-sedimentation of UCM05 in the same experiment, obtained measuring the absorbance at 315 nm. (E) Radial scans showing the sedimentation of FtsZ plus UCM05 with 200 μM GDP added. (F) Corresponding radial scans of UCM05 in the same experiment, showing a lack of co-sedimentation of the ligand. All of these experiments were performed in 50 mM Hepes-KOH, 50 mM KCl, 1 mM EDTA, 10 mM $MgCl_2$, pH 6.8 at 25 °C.

dx.doi.org/10.1021/cb400208z | *ACS Chem. Biol.* 2013, 8, 2072−2083

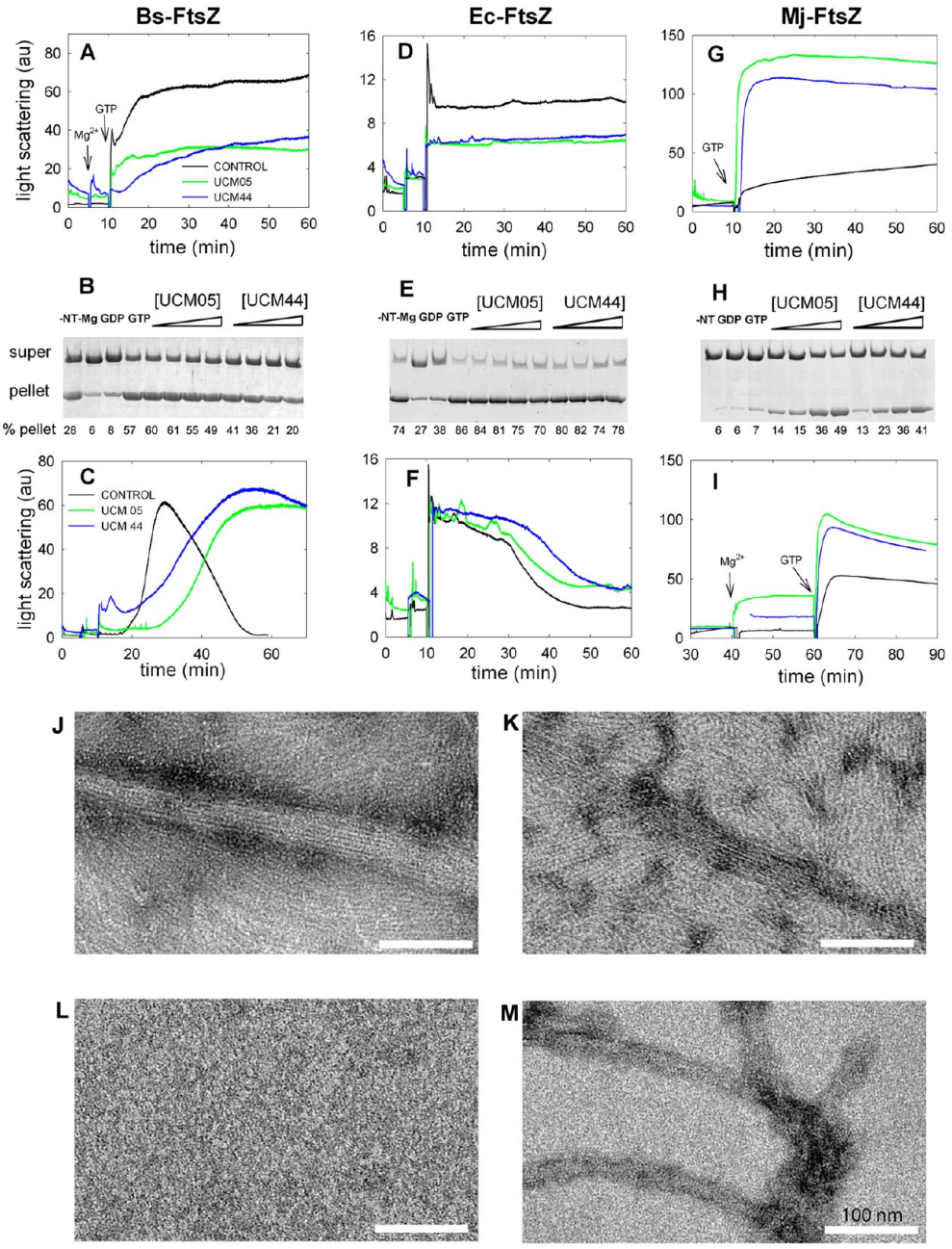

Figure 4. Effects of UCM05 and UCM44 on assembly of bacterial Bs-FtsZ, Ec-FtsZ, and archaeal Mj-FtsZ. The solution conditions were adjusted for each FtsZ species (Methods). (A) Light scattering time courses of 10 μM Bs-FtsZ polymerization with a GTP regenerating system (RS) at 25 °C. Black line, control containing 2% DMSO and Bs-FtsZ. Green line, with 20 μM UCM05. Blue line, with 20 μM UCM44. $MgCl_2$ (10 mM) and GTP (50 μM) were added at 5 and 10 min, respectively, indicated by the arrows. (B) Sedimentation assays of Bs-FtsZ polymer formation with GTP RS. Assembly was allowed to proceed for 15 min before polymer pelleting by centrifugation at 25 °C. Controls without nucleotide (-NT), without Mg^{2+} (-Mg), with GDP (1 mM, no RS), and with GTP RS (no ligand) are shown on the first 4 lanes. The effects of increasing concentrations of each ligand, 10, 20, 40, and 50 μM UCM05 or UCM 44, are shown in the next 8 lanes. The percent protein in the pellet is indicated below each lane. (C) Light-scattering time courses of Bs-FtsZ polymerization-depolymerization with 1 mM GTP and no RS, 1% DMSO (otherwise as in panel A). (D–F) Experiments with Ec-FtsZ similar to panels A–C, but at 30 °C (with 12 μM Ec-FtsZ in panels D and F, 8 μM Ec-FtsZ in panel E, and 60 μM GTP in panels D and E). Note that purified Bs-FtsZ and Ec-FtsZ have bound guanine nucleotide (Supplementary Information). (G–I) Corresponding experiments with 9 μM Mj-FtsZ (nucleotide free) at 40 °C, with 40 μM UCM05 or UCM44 (2% DMSO) in panels G and I (Methods). In panel G, GTP was added to the Mg^{2+}-containing samples at 10 min. The concentrations of UCM05 and UCM44 in panel H are 10, 20, 30, and 50 μM. In panel I, Mg^{2+} was added at 40 min and GTP at 60 min. EM of Bs-FtsZ (J) with GTP RS, (K) with GTP RS and 20 μM UCM44, (L) without nucleotide, and (M) with 40 μM UCM44.

at the tight interface between monomers,[5,6,25] raising the possibility that the nucleotide accessibility in the FtsZ filament may differ between species. Therefore we have determined the effects of UCM05 and UCM44 on the assembly of three different FtsZ from a Gram-positive bacterium (Bs-FtsZ), a Gram-negative bacterium (Ec-FtsZ), and an archaea (Mj-FtsZ), employing light scattering, polymer sedimentation, electron microscopy (EM), and GTPase methods.

dx.doi.org/10.1021/cb400208z | ACS Chem. Biol. 2013, 8, 2072–2083

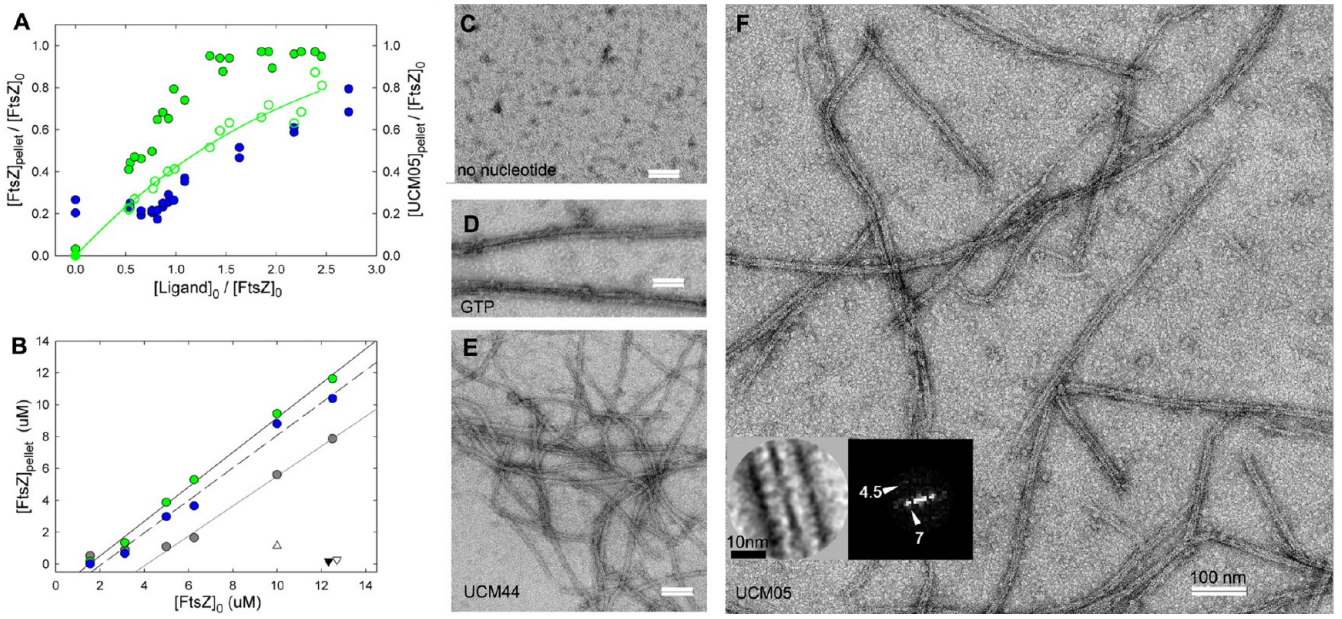

Figure 5. Ligand-induced Mj-FtsZ filament assembly. (A) Sedimentation of polymers formed by Mj-FtsZ (10 μM nucleotide-devoid protein at 40 °C; Methods) with increasing concentrations of UCM05 (green dots) or UCM44 (blue dots). The void symbols are the UCM05 co-sedimented with the protein, and the green line is a best fitting binding isotherm of 1.4 ± 0.3 UCM05 molecules per FtsZ with an apparent affinity of (6.9 ± 2.0) × 10^4 M^{-1}. (B) Quantification of ligand-induced polymers at varying protein concentrations: UCM05 (30 μM), green dots; UCM44 (30 μM), blue dots; GTP (1 mM), gray dots. Least squares regression lines are shown. Control with GDP (1 mM), solid triangle; without ligand or nucleotide, open inverted triangle; with UCM05 but without Mg^{2+}, open triangle. Negatively stained EM of Mj-FtsZ (9 μM) (C) without ligand or nucleotide, (D) with GTP. Representative micrograph (E) with UCM44 and (F) with UCM05. The white bars in each panel correspond to 100 nm. The left inset in panel F is an average image from 159 aligned segments of the UCM05-induced polymers, and the right inset its computed diffractogram. UCM44-induced polymers gave similar results.

UCM05 or UCM44 (20 μM) reduced the scattering increment and the amount of sedimentable polymer upon assembly of Bs-FtsZ (10 μM), with a GTP (50 μM) regenerating system (RS) employed to maintain a low nucleotide concentration and a high GTP/GDP ratio (Figure 4A,B). Similar experiments with 1 mM GTP (without RS) showed reduced assembly and disassembly rates in comparison with the control (Figure 4C). Note that the assembly experiments with 1 mM GTP are employed to check reversibility (disassembly upon nucleotide consumption) but are less favorable for competing ligands than experiments with 50 μM GTP RS. Negative stain EM showed a reduction in the formation of the characteristic filament bundles formed by Bs-FtsZ with GTP (Figure 4J,K) and GTP RS (Supplementary Figure S4). With a larger excess of UCM05 or UCM44 (40 μM) and initially no GTP, we observed a Mg^{2+}-dependent light scattering increase with formation of disordered polymers and aggregates (Figure 4L,M). UCM05 was not hydrolyzed by Bs-FtsZ (determined by HPLC) and inhibited ∼50% of its GTPase activity (Supplementary Figure S5). Putting together these results we concluded that UCM05 and UCM44 binding impairs the normal assembly of Bs-FtsZ protofilaments and leads to disordered polymerization, probably by distorting the Bs-FtsZ self-association interface. We hypothesize that the ligand-induced dimerization detected by sedimentation velocity (above) is a first step of incorrect polymerization induced by these ligands that replace GTP.

These compounds reduced the light scattering increase during Ec-FtsZ assembly with GTP RS (Figure 4D), weakly reduced polymer pelleting (Figure 4E), and did not reduce scattering with 1 mM GTP (no RS) (Figure 4F). A reduction in the lateral association of Ec-FtsZ filaments with UCM05 and UCM44 with respect to the controls was appreciated by EM (Supplementary Figure S4). A weak (≤20%) inhibition of the GTPase activity was also observed (Supplementary Figure S5). Therefore, we considered these compounds weak inhibitors of Ec-FtsZ assembly.

Recently, GTPase activity assays in the presence and absence of Triton X-100 (0.01% v/v, near the critical micelle concentration CMC ≈ 0.02% v/v) have been employed to compare 9 FtsZ inhibitors and identify 4 aggregators.[35] This neutral detergent disrupts aggregates of promiscuous small molecules that nonspecifically inhibit enzymes.[45] However, we have observed that Triton X-100 also inhibits assembly of bacterial Bs-FtsZ and Ec-FtsZ (Supplementary Figure S6) and interferes in EM forming large micellar FtsZ condensates (Supplementary Figure S7), which prevented us from meaningfully adding this detergent to the experiments with FtsZ assembly inhibitors. Actually, a substantial part of the protein−protein interactions in FtsZ polymers involve hydrophobic areas[3,46] expected to bind detergent. In fact, Triton X-100 and other mild detergents, at concentrations near their CMCs, massively bind to FtsZ's eukaryotic homologue tubulin, modifying its structure and assembly.[47−49] These pieces of evidence cast doubt on using Triton X-100 to distinguish specific from aggregation-based ligand effects on protein assembly systems such as FtsZ.

Ligand-Induced Assembly of Archaeal FtsZ. The effects of UCM05 and UCM44 on the assembly of archaeal Mj-FtsZ were very different from bacterial FtsZ. Both compounds together with GTP RS induced a large increase in light scattering (Figure 4G) and also in sedimentable polymer (Figure 4H) with respect to the controls with GTP. We also observed a rapid, stable, Mg^{2+}-dependent increase in scattering

dx.doi.org/10.1021/cb400208z | ACS Chem. Biol. 2013, 8, 2072−2083

induced by UCM05 or UCM44 alone, followed by a larger increase after 1 mM GTP addition (Figure 4I). However, the gross EM morphology of the polymers and the GTPase activity (Supplementary Figure S5) were not significantly modified. It is noteworthy that using just one method, in particular GTPase activity,[35] or a single FtsZ species, the effects observed would have been misleading. These results suggested that UCM05 and UCM44 could be acting as nonhydrolyzable surrogates of GTP in Mj-FtsZ assembly, and we thus proceeded to characterize the polymers induced by these ligands.

Measurements of the formation of nucleotide-devoid Mj-FtsZ polymers with increasing UCM05 concentrations were compatible with the binding of one ligand molecule per FtsZ (Figure 5A). The ligand-induced polymerization of Mj-FtsZ proceeded above a critical concentration (Cr, Figure 5B), indicating a nucleated condensation mechanism.[50] The Cr values, 1.5 μM with UCM05 and 2.1 μM with UCM44, showed a more efficient polymerization with these ligands, which were not hydrolyzed by Mj-FtsZ (quantified by HPLC), than with GTP (Cr = 4.1 μM). The Mj-FtsZ polymers induced by GTP were characteristic filamentous bundles in negative stain EM (Figure 5D).[46,51] However, most polymers induced by UCM44 and UCM05 were distinct, better defined filaments (Figure 5E,F, respectively), which we had not seen before. These filaments reach several micrometers in length, are ~15 nm wide, typically have less dense zones along their axis, and in some cases show a twisted appearance. They are clearly different from the basic structure formed by Mj-FtsZ with GTP or with the slowly hydrolyzable analogue GMPCPP, which is a ~8 nm wide filament made of two parallel protofilaments in close contact.[51,52] They are also different from the Bs-FtsZ bundles induced by the antibacterial compound PC190723, in which the lateral spacing between protofilaments is 3.8 nm.[28] An average image and computed diffractogram of the UCM05-induced polymers (Figure 5F, insets; similar results were obtained with UCM44) are preliminarily compatible with one of two possibilities: (i) a pair of FtsZ protofilaments laterally spaced 7 nm (giving the equatorial diffraction spot at 1/7 nm^{-1}) that would be bridged in a nonevident manner and would have a calculated width of only 11−12 nm according to the dimensions of an FtsZ molecule and (ii) the projection image of hollow tubes of ~8.5 nm mean diameter, which would have 5−7 monomers per turn and a calculated external diameter of 12−13.5 nm that is closer to the observed ~15 nm width. In this second case the diffraction corresponds to the Fourier transform of a hollow cylinder, and the equatorial spot is assumed to be the first subsidiary extreme of a zero-order Bessel function, which is located at ~1.22 times the reciprocal value of the mean cylindrical diameter.[53] The position of the first layer line in the diffractogram corresponds to the typical 4.5 nm spacing between FtsZ monomers along protofilaments, irrespective of the model. The UCM05 fragments UCM16 and UCM17 also induced Mj-FtsZ polymerization, although with higher Cr values and forming wider twisted bundles (Supplementary Figure S8).

We concluded from these results that UCM05 and UCM44 induce Mj-FtsZ assembly, possibly by fitting into the nucleotide site at the association interface between Mj-FtsZ monomers. This may involve some structural rearrangement with respect to GTP, leading to tubule-like FtsZ polymers that are worth further biophysical investigation. These polymers do not disassemble and would lack the physiological dynamics necessary for cell division. We do not rule out a similar suppression of dynamics of Bs-FtsZ polymers. However, in this case the ligands may not fit easily into a tighter association interface between monomers in bacterial FtsZ filaments, leading to more drastically altered protein−protein contacts and the observed formation of disordered polymers or aggregates, even with GTP in the medium, thus impairing normal FtsZ filaments. Note that UCM05 and UCM44 competitively inhibit the binding of GTP (Figures 1 and 2), and their binding is abolished by nucleotide (Figure 3). Structural confirmation of how these ligands replace GTP by binding into FtsZ's nucleotide site (instead of allosterically inhibiting GTP binding) would be valuable for inhibitor design.

Structural Insights from FtsZ-Inhibitor Model Complexes. In order to analyze the potential binding modes of the inhibitors to FtsZ, we employed the 1.7 Å crystal structure of nucleotide devoid Bs-FtsZ. As a proof of concept and reference state, we first docked a GDP molecule to the nucleotide site of this apo-FtsZ structure and subsequently validated the docking results with molecular dynamics (MD). The results were in full agreement with the Bs-FtsZ-GDP crystal structure and with a previous computational analysis.[34] The binding site is relatively flexible, and GDP fluctuated within the site 1 Å on average (Supplementary Figure S9A), the largest movements being linked to loop T3 and the N-terminal end of helix H7. Despite this flexibility, many of the crystallographic interactions observed in a GDP liganded structure were stable along the 100 ns of MD simulation. As described before,[34] the GDP phosphates interact with the glycine-rich loops T4 and T1, the guanine ring stacks between helix H7(Phe183) and H1, and the ribose interacts electrostatically with T5, in addition to sharing the interaction with Phe183. We tackled the plasticity of the nucleotide-binding site with advanced multireceptor docking approaches,[54] in particular the ICM 4D docking protocol that considers multiple receptor conformers as an extra dimension for the docking search.[55] The conformational variability of the nucleotide-binding site was represented with seven conformers extracted from different snapshots of a long MD simulation of the apo-FtsZ structure. These discrete conformers were simultaneously and efficiently considered in every single docking experiment. The best docking solutions obtained for each UCM ligand were subjected to MD simulations to confirm the ligand stability in the nucleotide-binding site. The UCM ligands fluctuated in the binding site similarly to GDP (Supplementary Figure S9). In these models UCM05 and UCM44 interact with FtsZ's nucleotide site in a similar fashion, but we identify two different, similarly probable binding modes. Representative MD snapshots of the first binding mode of UCM05 and UCM44 superimposed with GDP-FtsZ are shown by Figure 6A,B, respectively. In this binding mode, the naphthalene ring binds in a hydrophobic pocket between helices H7 and H5 and the sugar recognition loop T5. The 1-polyhydroxybenzoyl arm interacts with helix H7, whereas the 3-polyhydroxybenzoyl arm binds between loops T4 and T1. These two binding regions roughly correspond to the nucleobase- and phosphate-binding locations, respectively. In the second binding mode the naphthalene points deeper into the protein, the ligand is reversed, and the 1-polyhydroxybenzoyl arm is more exposed, interacting with T1, T4, and T5 (Supplementary Figure S10). Figure 6C shows the protein−ligand interactions and binding pocket characteristics for the first binding mode of UMC44. This 2D representation highlights the main model interactions with nearest amino acids. The key residues for GDP binding are marked with

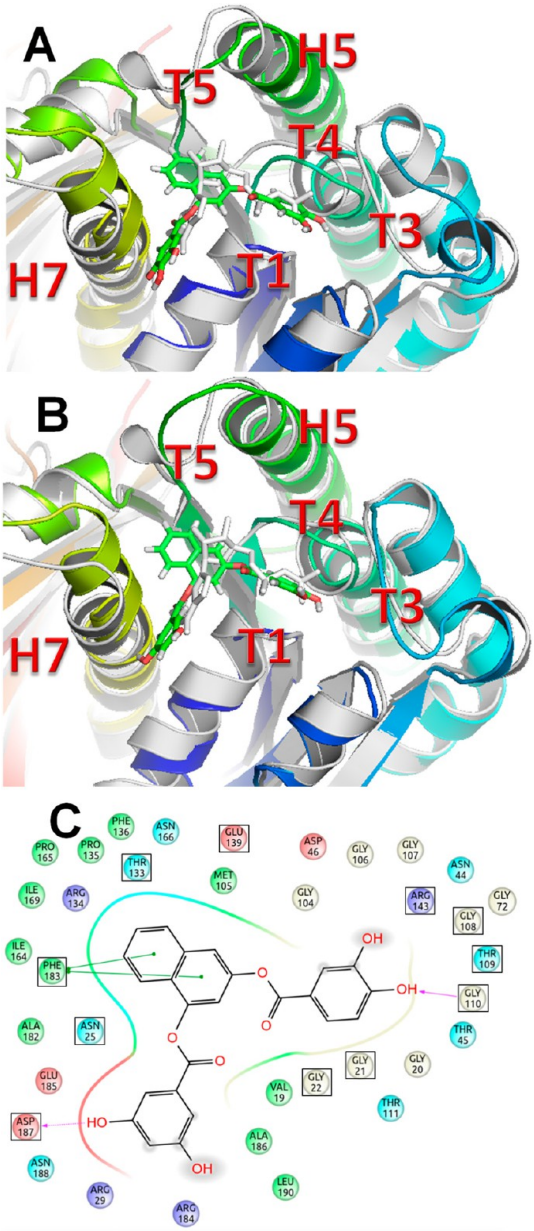

Figure 6. Representative snapshots of the MD simulation for first binding mode of UCM05 (A) and UCM44 (B) (colored) superimposed with the GDP-bound crystallographic structure (gray). (C) Ligand interaction diagram of residues located in the UCM44 binding site (≤5 Å from the ligand). The amino acid color stands for hydrophobic (green), glycine (gray), polar (light blue), positively charged (magenta), and negatively charged (red). The magenta arrows represent H-bonds, and green lines correspond to $\pi-\pi$ interactions. The shadowed atoms indicate solvent exposure.

squares (for details of interactions found in MD simulations for both binding modes see Supplementary Tables S1 and S2). Although it is not possible to rule out other ligand-binding poses that may escape our modeling approach, the interactions in common between GDP and the ligand model complexes outline a potential inhibition mechanism, to be tested by synthetic and structural experiments. On the other hand, docking experiments of monomer structures are unlikely to explain why UCM05 and UCM44 perturb Bs-FtsZ but induce Mj-FtsZ assembly since the structure elements in the binding site are almost identical. We expect that such differences will be related with the filament dynamics and how these compounds affect the possibly different polymerization interfaces between bacterial and archaeal FtsZ monomers.

Impairment of the Z-Ring, Inhibition of Cell Division, and Antibacterial Activity. We observed that UCM05, UCM44, and UCM53 induce filamentation of *B. subtilis* cells, indicating inhibition of cell division, at concentrations below their MICs (Figure 7A). UCM05 was not appreciably hydrolyzed by the bacterial cultures in 2 and 4 h, and 60% of it remained after 18 h (quantified by HPLC). Visualizing the Z-ring in *B. subtilis* SU570 cells, which contain fused FtsZ-GFP as the only FtsZ protein,[56] showed that these compounds induce FtsZ delocalization with formation of numerous punctuate foci and distorted ring structures (Figure 7B; statistics are plotted in Supplementary Figure S11). Control cells had FtsZ rings (0.139 ± 0.003 ring/μm) and few FtsZ foci (0.072 ± 0.015 foci/μm). In the presence of UCM05 (40 μM) cells had more ring-like structures (0.242 ± 0.024 per μm) and more foci (0.443 ± 0.070 per μm). Similar results were obtained with UCM44 (12 μM; 0.178 ± 0.022 rings/μm; 0.439 ± 0.036 foci/μm). In contrast UCM53 (3 μM) induced a reduction in rings (0.050 ± 0.010 per μm) and an increase of foci (0.128 ± 0.025 per μm). These results clearly indicate a functional impairment of FtsZ, although indirect effects via FtsZ-interacting partners cannot be totally excluded,[22] and we have observed a reduction in nucleoid size with UCM05 and UCM44, whereas UCM53 has a nucleoid extension effect (Figure 7B).

The antibacterial profile of these small molecules (Table 1) has shown growth-inhibitory activity on several Gram-positive pathogens more than on Gram-negative bacteria. The MIC values systematically follow the order UCM05 > UCM44 > UCM53, the later reaching one-digit (mg/L) numbers. UCM53 is active on methicillin-resistant *Staphylococcus aureus*, ampicillin- and levofloxacin-resistant *Enterococcus faecium*, and levofloxacin-resistant *Enterococcus faecalis* and weakly active on *Streptococcus pneumoniae*. The three compounds were equally active against the antibiotic-sensitive and -resistant clinical isolates tested, including weak activities on Gram-negative *Acinetobacter baumanii* and *Pseudomonas aeruginosa* (Table 1) and weak bactericidal activities on *S. aureus* and *S. pneumoniae* (Supplementary Table S3).

These compounds inhibit mammalian cells growth at concentrations (Supplementary Table S4) partially overlapping the bacterial MICs. However, the antibacterial selectivity (IC_{50}/MIC) markedly improves when going from UCM05 to UCM44 and to UCM53. Thus the IC_{50} values of UCM53 on normal (HUVEC, IMR90, MDCK, 3T3) and tumor cell lines (A549, 3T3-SV40, Hs57T, A2780, HeLa) are 2−12-fold higher than the MIC on *S. aureus* and 8−47-fold higher than the *E. faecalis* MIC (Supplementary Table S5). On the other hand, the compounds lacked significant effects on the cytoplasmic microtubules of A549 cells and did not induce the accumulation of mitotic cells in the G2/M phase of the cell cycle typical of microtubule inhibitors (Supplementary Figure S12). From these results we concluded that the growth inhibition by these compounds is not specific to microtubules. Although high concentrations (100 μM) of UCM05 and UCM53 inhibited the assembly of purified tubulin into microtubules, UCM44 inhibited to a lesser extent and UCM16 and UCM17 had no effect (Supplementary Figure S13). New analogues containing the essential chemical features for binding, which are being investigated, selectively inhibit FtsZ. These features, supported by the low animal toxicity of UCM05 (>70 mg/kg daily [40]),

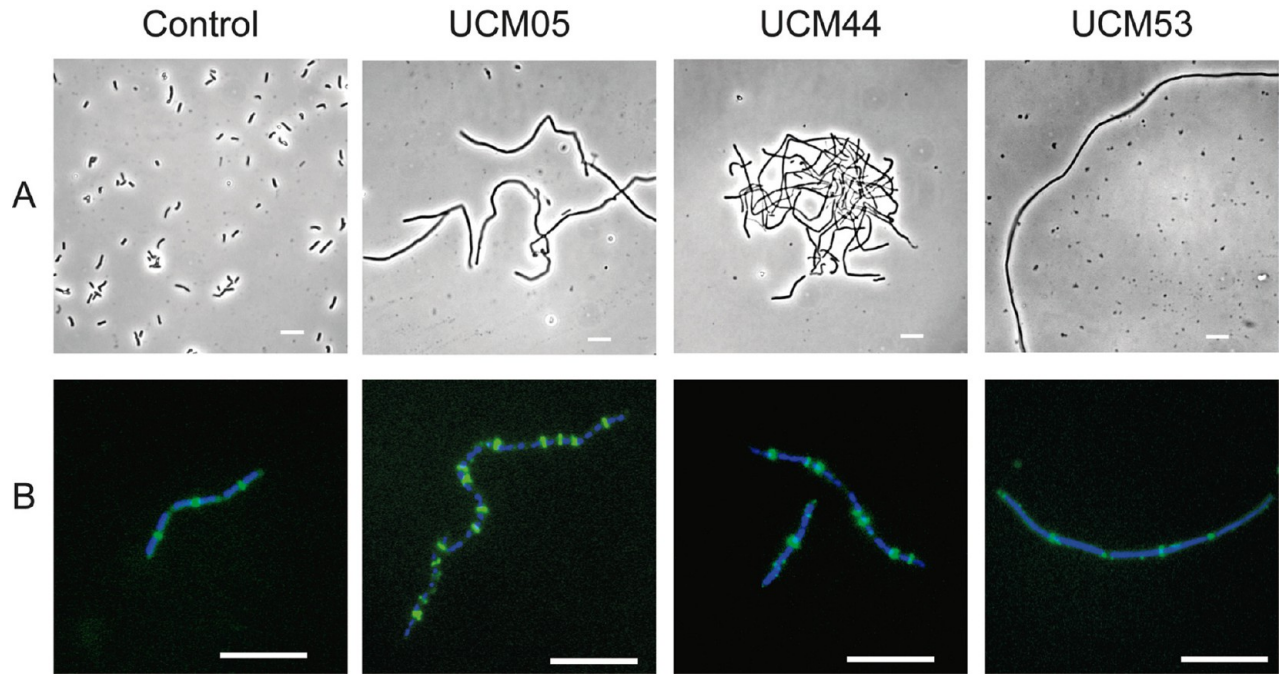

Figure 7. *In vivo* effects of UCM05, UCM44, and UCM53 on *B. subtilis* cells. (A) *B. subtilis* 168 cells after 2 h of culture at 37 °C with UCM05 (50 μM), UCM44 (12 μM), or UCM53 (12 μM) observed by phase-contrast microscopy. (B) Cells of *B. subtilis* SU570, in which the wild type *ftsZ* gene is replaced by *ftsZ-gfp*, were incubated during 1 h at 30 °C with UCM05 (40 μM), UCM44 (12 μM), or UCM53 (3 μM), FtsZ-GFP (green) and DNA stained with DAPI (blue), visualized with fluorescence microscopy. Scale bars, 10 μm.

Table 1. Inhibition of Bacterial Cell Growth. MIC (mg/L)[a]

microorganism	UCM05	UCM44	UCM53
B. subtilis 168[b]	64	16	4
S. aureus methicillin-S ATCC 29213	32	16	8
S. aureus methicillin-R 12160636	32	16	8
E. faecium ampicillin-R and levofloxacin-R 12160560	64	32	4
E. faecalis ATCC 29212	64	32	2
E. faecalis levofloxacin-R 12165475	64	32	4
S. pneumoniae ATCC 49619	64	32	32
S. pneumoniae penicillin-S 12161018	64	64	32
S. pneumoniae penicillin-R 12159853	64	64	32
A. baumannii multi-R 12159796	64	64	32
P. aeruginosa ATCC27853	128	64	64
P. aeruginosa imipenem-R 12161227	128	64	64
E. cloacae multi-R 12161389	128	128	128
E. coli ATCC 35218	128	128	128
K. pneumoniae ESBL[c] ATCC 700603	128	128	128

[a]Minimal concentrations completely inhibiting bacterial growth (MIC) were determined by microdilution assays, except as noted. [b]Average of microdilution and previous tube assays. The non-ATCC strains employed are clinical isolates susceptible (S) or resistant (R) to antibiotics commonly used for the treatment of infections produced by these species. [c]ESBL: extended-spectrum β-lactamase.

suggest the possibility of further improving the antibacterial selectivity of these model compounds.

Conclusions. In this work we have successfully replaced the natural GTP regulator of cell division protein FtsZ with nonsubstrate synthetic ligands UCM05, UCM44, and UCM53 that competitively inhibit GTP binding. Model binding modes of UCM05 and UCM44 explain the inhibitor character of these compounds, whose phenolic groups and naphthalene scaffold may be predicted to replace interactions made by the phosphates and the nucleobase of GTP. They act as interfacial modifiers of FtsZ assembly, rather than as competitive protein–protein interaction inhibitors. This leads to functional inhibition of bacterial FtsZ filaments. In the case of archaeal FtsZ, these ligands induce the assembly of distinct tubule-like polymers.

These small molecules targeting FtsZ effectively impair the Z-ring assembly in bacterial cells, and the analogue UCM53 effectively inhibits the growth of Gram-positive pathogens. They practically lack effect on Ec-FtsZ, similarly to the situation encountered with the antimicrobial compound PC190723.[24,26,28] However, given the strong conservation of the nucleotide-binding site among different FtsZ[44] and the weak effect observed on some Gram-negative pathogens, it may be feasible to obtain effective GTP-replacing inhibitors for Gram-negative FtsZ proteins as well.

How these ligands inhibit the FtsZ function *in vivo* by binding to the nucleotide site appears puzzling: since their affinity for FtsZ monomers is 1 order of magnitude lower than GTP, and the concentration of GTP in the bacterial cytosol is on the order of millimolar,[57] if the inhibitor reached an intracellular concentration of 100 μM, about 1 in 100 FtsZ molecules would bind the ligand. However, it is possible that the contacts with the next monomer along the filament may substantially increase the ligand affinity relative to GTP. In addition, the repetitive nature of protein self-assemblies makes them quite susceptible to substoichiometric inhibition by binding to a few subunits per polymer, which disrupt its structure or impair the assembly disassembly dynamics required for its cellular function. A classic example is the inhibition of microtubule dynamics by antitumor drugs.[58]

The results obtained with these model compounds constitute a first systematic approach to the FtsZ nucleotide site as an antibacterial target. While writing this paper we have

determined that a chemically related synthetic fragment of the natural marine compound crysophaentin A from the Bewley laboratory (compound 11)[59] also competes with GTP for binding to FtsZ.[60] We also note different, positively charged diphenylnaphthalene antibacterial compounds aimed at FtsZ.[61] Current challenges for developing cell division inhibitors targeting the GTP-binding site of FtsZ into antibacterial agents include determining the atomic structures of FtsZ-inhibitor complexes, exploring other chemical structures, and optimizing the affinity for the FtsZ polymerization interface and antibacterial activity.

METHODS

Chemistry. The synthesis and spectroscopic data of compound **2** (UCM05, Figure 1) were as reported previously.[40] Full synthetic details as well as characterization data of compounds **3**–**6** and PC170942,[14] together with synthesis of all intermediates, are described in the Supporting Information (Schemes S1 and S2). Spectral characterization data of all described compounds were consistent with the proposed structures. Compounds **2**–**6** and PC170942 were >95% pure by HPLC-MS (Supplementary Table S6).

VS compounds (Supplementary Table S7) were purchased from Enamine, Interchim, InterBioScreen, and Life Chemicals. Mant-GTP was from Jena Bioscience, and ^{3}H-GTP was from Perkin-Elmer. Other chemicals were from Sigma.

Small Molecule Solubility in Aqueous Buffer. Synthetic compounds were carefully weighed and dissolved (50 mM) in spectroscopy grade dimethyl sulfoxide (DMSO). The stock solutions were kept dry at −20 °C or −75 °C. They were gravimetrically diluted into DMSO and then at increasing concentrations, starting from the low micromolar range, into 50 mM Hepes/KOH, 50 mM KCl, 1 mM EDTA, pH 6.8 buffer, with 2% residual DMSO. Their absorption spectra were acquired above 240 nm, using microcuvettes of several optical paths with a Evolution 300 spectrophotometer (Thermo) calibrated with absorption standards. The linearity of absorption versus concentration was checked, as well as any light scattering at wavelengths above the absorption bands indicating precipitation. The extinction coefficients determined in buffer for selected compounds were UCM05, 24000 ± 900 M^{-1} cm^{-1} at 286 nm maximum (shoulder at 336 nm, ∼5400 M^{-1} cm^{-1}); UCM44, 16300 ± 800 M^{-1} cm^{-1} at 260 nm (shoulder at 295 nm); UCM53, 6700 ± 540 M^{-1} cm^{-1} at 312 nm. The more concentrated solutions in which the compounds were apparently soluble were centrifuged at 386,000*g* for 20 min in a TLA100 rotor (100,000 rpm) at 25 °C with a Beckman TLX table-top ultracentrifuge, and their absorption spectra recorded again. The compound concentration remaining in the supernatant was considered for practical purposes the solubility limit of each free ligand in buffer. These values were approximately: UCM05, 50 μM; UCM44, 30 μM; UCM53, 5 μM; UCM16, >120 μM; UCM17, >120 μM; VS2.18, >500 μM; PC170942, 15 μM. UCM05 and UCM44 remained similarly soluble under the conditions of the *mant*-GTP competition assay with 0.5 μM Bs-FtsZ. Ligands effective solubility increased by binding to FtsZ or in culture media.

ASSOCIATED CONTENT

Supporting Information

Computational, biochemical, and biological methods. Molecular dynamics simulations, docking and VS, proteins purification, ligand competition with ^{3}H-GTP and with *mant*-GTP for binding to FtsZ, difference absorption spectroscopy, analytical ultracentrifugation, light scattering, electron microscopy, FtsZ polymer sedimentation, GTPase activity, ligand binding to FtsZ polymers, compound stability, antibacterial activity, bacterial division phenotype, FtsZ-GFP localization, mammalian cell culture, cell growth inhibition, microtubule visualization, and cell cycle methods. Supplementary Tables S1 to S3, supplementary Figures S1 to S7, four supplementary files in PDB format. These materials are available free of charge via the Internet at http://pubs.acs.org.

AUTHOR INFORMATION

Corresponding Author

*E-mail: j.m.andreu@cib.csic.es.

Notes

The authors declare no competing financial interest.

ACKNOWLEDGMENTS

We thank E. J. Harry and M. P. Strauss for *B. subtilis* strain SU570, D. Juan for FtsZ purification, R. Nuñez-Ramirez for the image analysis in Figure 5, O. Llorca for EM advice, and J. M. Sanchez-Puelles for discussion. This work was supported by grants from Plan Nacional de Investigación BFU 2011-23416 (J.M.A.), BFU2099-09552 (P.C.), and SAF2010-22198 (M.L.L.-R.), grant CM S2010/BMD-2353 (M.L.L.-R, P.C., J.M.A.), and fellowships FPI (L.B.R.-A.), FPU (M.A.) and CSIC-JAE (E.R.-A.).

REFERENCES

(1) Adams, D. W., and Errington, J. (2009) Bacterial cell division: assembly, maintenance and disassembly of the Z ring. *Nat. Rev. Microbiol. 7*, 642–653.

(2) Egan, A. J. F., and Vollmer, W. (2013) The physiology of bacterial cell division. *Ann. N.Y. Acad. Sci. 1277*, 8–28.

(3) Nogales, E., Downing, K. H., Amos, L. A., and Lowe, J. (1998) Tubulin and FtsZ form a distinct family of GTPases. *Nat. Struct. Biol. 5*, 451–458.

(4) Oliva, M. A., Cordell, S. C., and Lowe, J. (2004) Structural insights into FtsZ protofilament formation. *Nat. Struct. Mol. Biol. 11*, 1243–1250.

(5) Elsen, N. L., Lu, J., Parthasarathy, G., Reid, J. C., Sharma, S., Soisson, S. M., and Lumb, K. J. (2012) Mechanism of action of the cell-division inhibitor PC190723: Modulation of FtsZ assembly cooperativity. *J. Am. Chem. Soc. 134*, 12342–12345.

(6) Matsui, T., Yamane, J., Mogi, N., Yamaguchi, H., Takemoto, H., Yao, M., and Tanaka, I. (2012) Structural reorganization of the bacterial cell-division protein FtsZ from Staphylococcus aureus. *Acta Crystallogr., Sect. D: Biol. Crystallogr. 68*, 1175–1188.

(7) Erickson, H. P., Anderson, D. E., and Osawa, M. (2010) FtsZ in bacterial cytokinesis: cytoskeleton and force generator all in one. *Microbiol. Mol. Biol. Rev. 74*, 504–528.

(8) Buske, P. J., and Levin, P. A. (2012) Extreme C terminus of bacterial cytoskeletal protein FtsZ plays fundamental role in assembly independent of modulatory proteins. *J. Biol. Chem. 287*, 10945–10957.

(9) Li, Z., Trimble, M. J., Brun, Y. V., and Jensen, G. J. (2007) The structure of FtsZ filaments in vivo suggests a force-generating role in cell division. *EMBO J. 26*, 4694–4708.

(10) Payne, D. J. (2008) Desperately seeking new antibiotics. *Science 321*, 1644–1645.

(11) Fischbach, M. A., and Walsh, C. T. (2009) Antibiotics for emerging pathogens. *Science 325*, 1089–1093.

(12) Boucher, H. W., Talbot, G. H., Bradley, J. S., Edwards, J. E., Gilbert, D., Rice, L. B., Scheld, M., Spellberg, B., and Bartlett, J. (2009) Bad bugs, no drugs: No ESKAPE! An update from the Infectious Diseases Society of America. *Clin. Infect. Dis. 48*, 1–12.

(13) Wang, J., Galgoci, A., Kodali, S., Herath, K. B., Jayasuriya, H., Dorso, K., Vicente, F., Gonzalez, A., Cully, D., Bramhill, D., and Singh, S. (2003) Discovery of a small molecule that inhibits cell division by blocking FtsZ, a novel therapeutic target of antibiotics. *J. Biol. Chem. 278*, 44424–44428.

(14) Stokes, N. R., Sievers, J., Barker, S., Bennett, J. M., Brown, D. R., Collins, I., Errington, V. M., Foulger, D., Hall, M., Halsey, R., Johnson, H., Rose, V., Thomaides, H. B., Haydon, D. J., Czaplewski, L. G., and Errington, J. (2005) Novel inhibitors of bacterial cytokinesis identified

by a cell-based antibiotic screening assay. *J. Biol. Chem. 280*, 39709−39715.
(15) Serbus, L. R., Landmann, F., Bray, W. M., White, P. M., Ruybal, J., Lokey, R. S., Debec, A., and Sullivan, W. (2012) A cell-based screen reveals that the albendazole metabolite, albendazole sulfone, targets Wolbachia. *PLoS Path. 8*, No. e1002922.
(16) Tsao, D. H. H., Sutherland, A. G., Jennings, L. D., Li, Y., Rush, T. S., III, Alvarez, J. C., Ding, W., Dushin, E. G., Dushin, R. G., Haney, S. A., Kenny, C. H., Malakian, A. K., Nilakantan, R., and Mosyak, L. (2006) Discovery of novel inhibitors of the ZipA/FtsZ complex by NMR fragment screening coupled with structure-based design. *Biorg. Med. Chem. 14*, 7953−7961.
(17) Sass, P., Josten, M., Famulla, K., Schiffer, G., Sahl, H. G., Hamoen, L., and Brotz-Oesterhelt, H. (2012) Antibiotic acyldepsipeptides activate ClpP peptidase to degrade the cell division protein FtsZ. *Proc. Natl. Acad. Sci. U.S.A. 108*, 17474−17479.
(18) Ghosal, A., Vitali, A., Stach, J. E., and Nelsen, P. E. (2012) Role of SbmA in the uptake of peptide nucleic acid (PNA)-peptide conjugates in *E. coli*. *ACS Chem. Biol. 8*, 360−367.
(19) Löwe, J., and Amos, L. A. (1998) Crystal structure of the bacterial cell-division protein FtsZ. *Nature 391*, 203−206.
(20) Vollmer, W. (2006) The prokaryotic cytoskeleton: a putative target for inhibitors and antibiotics? *Appl. Microbiol. Biotechnol. 73*, 37−47.
(21) Lock, R. L., and Harry, E. J. (2008) Cell-division inhibitors: new insights for future antibiotics. *Nat. Rev. Drug Discovery 7*, 324−338.
(22) Foss, M. H., Eun, Y. J., and Weibel, D. B. (2011) Chemical-biological studies of subcellular organization in bacteria. *Biochemistry 50*, 7719−7734.
(23) Schaffner-Barbero, C., Martin-Fontecha, M., Chacon, P., and Andreu, J. M. (2012) Targeting the assembly of bacterial cell division protein FtsZ with small molecules. *ACS Chem. Biol. 7*, 268−276.
(24) Haydon, D. J., Stokes, N. R., Ure, R., Galbraith, G., Bennett, J. M., Brown, D. R., Baker, P. J., Barynin, V. V., Rice, D. W., Sedelnikova, S. E., Heal, J. R., Sheridan, J. M., Aiwale, S. T., Chauhan, P. K., Srivastava, A., Taneja, A., Collins, I., Errington, J., and Czaplewski, L. G. (2008) An inhibitor of FtsZ with potent and selective anti-staphylococcal activity. *Science 321*, 1673−1675.
(25) Tan, C. M., Therien, A. G., Lu, J., Lee, S. H., Caron, A., Gill, C. J., Lebeau-Jacob, C., Benton-Perdomo, L., Monteiro, J. M., Pereira, P. M., Elsen, N. L., Wu, J., Deschamps, K., Petcu, M., Wong, S., Daigneault, E., Kramer, S., Liang, L. Z., Maxwell, E., Claveau, D., Vaillancourt, J., Skorey, K., Tam, J., Wang, H., Meredith, T. C., Sillaots, S., Wang-Jarantow, L., Ramtohul, Y., Langlois, E., Landry, F., Reid, J. C., Parthasarathy, G., Sharma, S., Baryshnikova, A., Lumb, K. J., Pinho, M. G., Soisson, S. M., and Roemer, T. (2012) Restoring methicillin-resistant Staphylococcus aureus susceptibility to beta-lactam antibiotics. *Sci. Trans. Med. 4*, No. 126ra35.
(26) Stokes, N. R. (2013) An improved small-molecule inhibitor of FtsZ with superior in vitro potency, drug-like properties and in vivo efficacy. *Antimicrob. Agents Chemother. 57*, 317−325.
(27) Adams, D. W., Wu, L. J., Czaplewski, L. G., and Errington, J. (2011) Multiple effects of benzamide antibiotics on FtsZ function. *Mol. Microbiol. 80*, 68−84.
(28) Andreu, J. M., Schaffner-Barbero, C., Huecas, S., Alonso, D., Lopez-Rodriguez, M. L., Ruiz-Avila, L. B., Nunez-Ramirez, R., Llorca, O., and Martin-Galiano, A. J. (2010) The antibacterial cell division inhibitor PC190723 is a FtsZ polymer stabilizing agent which induces filament assembly and condensation. *J. Biol. Chem. 285*, 14239−14246.
(29) Martín-Galiano, A. J., Buey, R. M., Cabezas, M., and Andreu, J. M. (2010) Mapping flexibility and the assembly switch of cell division protein FtsZ by computational and mutational approaches. *J. Biol. Chem. 285*, 22554−22565.
(30) Huecas, S., Schaffner-Barbero, C., Garcia, W., Yebenes, H., Palacios, J. M., Diaz, J. F., Menendez, M., and Andreu, J. M. (2007) The interactions of cell division protein FtsZ with guanine nucleotides. *J. Biol. Chem. 282*, 37515−37528.
(31) Läppchen, T., Hartog, A. F., Pinas, V. A., Koomen, G. J., and den Blaauwen, T. (2005) GTP analogue inhibits polymerization and GTPase activity of the bacterial protein FtsZ without affecting its eukaryotic homologue tubulin. *Biochemistry 44*, 7879−7884.
(32) Läppchen, T., Pinas, V. A., Hartog, A. F., Koomen, G. J., Schaffner-Barbero, C., Andreu, J. M., Trambaiolo, D., Lowe, J., Juhem, A., Popov, A. V., and den Blaauwen, T. (2008) Probing FtsZ and tubulin with C8-substituted GTP analogs reveals differences in their nucleotide binding sites. *Chem. Biol. 15*, 189−199.
(33) Läppchen, T. (2007) Synthesis of GTP analogues and evaluation of their effect on the antibiotic target FtsZ and its eukaryotic homologue tubulin. PhD Thesis, University of Amsterdam.
(34) Schaffner-Barbero, C., Gil-Redondo, R., Ruiz-Avila, L. B., Huecas, S., Lappchen, T., den Blaauwen, T., Diaz, J. F., Morreale, A., and Andreu, J. M. (2010) Insights into nucleotide recognition by cell division protein FtsZ from a mant-GTP competition assay and molecular dynamics. *Biochemistry 49*, 10458−10472.
(35) Anderson, D. E., Kim, M. B., Moore, J. T., O'Brien, T. E., Sorto, N. A., Grove, C. I., Lackner, L. L., Ames, J. B., and Shaw, J. T. (2012) Comparison of small molecule inhibitors of the bacterial cell division protein FtsZ and identification of a reliable cross-species inhibitor. *ACS Chem. Biol. 7*, 1918−1928.
(36) Shoichet, B. K. (2006) Screening in a spirit haunted world. *Drug Discovery Today 11*, 607−615.
(37) Coan, K. E. D., Maltby, D. A., Burlingame, A. L., and Shoichet, B. K. (2009) Promiscuous aggregate-based inhibitors promote enzyme unfolding. *J. Med. Chem. 52*, 2067−2075.
(38) Lakowicz, J. (1999) *Principles of Fluorescence Spectroscopy*, 2nd ed., pp 302−303, Kluwer Academic/Plenum Publishers, New York.
(39) Totrov, M., and Abagyan, R. (1997) Flexible protein-ligand docking by global energy optimization in internal coordinates. *Proteins Suppl 1*, 215−220.
(40) Puig, T., Aguilar, H., Cufi, S., Oliveras, G., Turrado, C., Ortega-Gutierrez, S., Benhamu, B., Lopez-Rodriguez, M. L., Urruticoechea, A., and Colomer, R. (2009) A novel inhibitor of fatty acid synthase shows activity against HER2+breast cancer xenografts and is active in anti-HER2 drug-resistant cell lines. *Breast Cancer Res. 13*, R131.
(41) Kuntz, I. D., Chen, K., Sharp, K. A., and Kollman, P. A. (1999) The maximal affinity of ligands. *Proc. Natl. Acad. Sci. U.S.A. 96*, 9997−10002.
(42) Turrado, C., Puig, T., Garcia-Carceles, J., Artola, M., Benhamu, B., Ortega-Gutierrez, S., Relat, J., Oliveras, G., Blancafort, A., Haro, D., Marrero, P. F., Colomer, R., and Lopez-Rodriguez, M. L. (2012) New synthetic inhibitors of fatty acid synthase with anticancer activity. *J. Med. Chem. 55*, 5013−5023.
(43) Rivas, G., Lopez, A., Mingorance, J., Ferrandiz, M. J., Zorrilla, S., Minton, A. P., Vicente, M., and Andreu, J. M. (2000) Magnesium-induced linear self-association of the FtsZ bacterial cell division protein monomer—The primary steps for FtsZ assembly. *J. Biol. Chem. 275*, 11740−11749.
(44) Oliva, M. A., Trambaiolo, D., and Lowe, J. (2007) Structural insights into the conformational variability of FtsZ. *J. Mol. Biol. 373*, 1229−1242.
(45) Feng, B. Y., and Shoichet, B. K. (2006) A detergent-based assay for the detection of promiscuous inhibitors. *Nat. Protoc. 1*, 550−553.
(46) Huecas, S., and Andreu, J. M. (2003) Energetics of the cooperative assembly of cell division protein FtsZ and the nucleotide hydrolysis switch. *J. Biol. Chem. 278*, 46146−46154.
(47) Andreu, J. M. (1982) Interaction of tubulin with non-denaturing amphipiles. *EMBO J. 1*, 1105−1110.
(48) Andreu, J. M., Delatorre, J., and Carrascosa, J. L. (1986) Interaction of tubulin with octyl glucoside and deoxycholate. 2. Protein conformation, binding of colchicine ligands and micritubule assembly. *Biochemistry 25*, 5230−5239.
(49) Andreu, J. M., Deancos, J. G., Starling, D., Hodgkinson, J. L., and Bordas, J. (1989) A synchrotron X-Ray scattering characterization of purified tubulin assembly and of its expansion induced by mild detergent binding. *Biochemistry 28*, 4036−4040.
(50) Huecas, S., Llorca, O., Boskovic, J., Martin-Benito, J., Valpuesta, J. M., and Andreu, J. M. (2008) Energetics and geometry of FtsZ

polymers: Nucleated self-assembly of single protofilaments. *Biophys. J. 94*, 1796−1806.
(51) Oliva, M. A., Huecas, S., Palacios, J. M., Martin-Benito, J., Valpuesta, J. M., and Andreu, J. M. (2003) Assembly of archaeal cell division protein FtsZ and a GTPase-inactive mutant into double-stranded filaments. *J. Biol. Chem. 278*, 33562−33570.
(52) Lowe, J., and Amos, L. A. (1999) Tubulin-like protofilaments in Ca2+-induced FtsZ sheets. *EMBO J. 18*, 2364−2371.
(53) Matesanz, R., Rodriguez-Salarichs, J., Pera, B., Canales, A., Andreu, J. M., Jimenez-Barbero, J., Bras, W., Nogales, A., Fang, W. S., and Diaz, J. F. (2011) Modulation of microtubule interprotofilament interactions by modified taxanes. *Biophys. J. 101*, 2970−2980.
(54) Totrov, M., and Abagyan, R. (2008) Flexible ligand docking to multiple receptor conformations: a practical alternative. *Curr. Opin. Struct. Biol. 18*, 178−184.
(55) Bottegoni, G., Kufareva, I., Totrov, M., and Abagyan, R. (2009) Four-dimensional docking: a fast and accurate account of discrete receptor flexibility in ligand docking. *J. Med. Chem. 52*, 397−406.
(56) Strauss, M. P., Liew, A. T. F., Turnbull, L., Whitchurch, C. B., Monahan, L. G., and Harry, E. J. (2012) 3D-SIM Super Resolution Microscopy Reveals a Bead-Like Arrangement for FtsZ and the Division Machinery: Implications for Triggering Cytokinesis. *PLoS Biol. 10*, No. e1001389.
(57) Buckstein, M. H., He, J., and Rubin, H. (2008) Characterization of nucleotide pools as a function of physiological state in Escherichia coli. *J. Bacteriol. 190*, 718−726.
(58) Jordan, M. A., and Wilson, L. (2004) Microtubules as a target for anticancer drugs. *Nat. Rev. Cancer 4*, 253−265.
(59) Keffer, J. L., Hammill, J. T., Lloyd, J. R., Plaza, A., Wipf, P., and Bewley, C. A. (2012) Geographic variability and anti-staphylococcal activity of the chrysophaentins and their synthetic fragments. *Mar. Drugs 10*, 1103−1125.
(60) Keffer, J. L., Huecas, S., Hammill, J. T, Wipf, P., Andreu, J. M. and Bewley, C. A. (2013) Chrysophaentins are competitive inhibitors of FtsZ and inhibit Z-ring formation in live bacteria, *Bioorg. Med. Chem.*, in press.
(61) Zhang, Y. Z., Giurleo, D., Parhi, A., Kaul, M., Pilch, D. S., and LaVoie, E. J. (2013) Substituted 1,6-diphenylnaphtalenes as FtsZ-targeting antibacterial agents. *Bioorg. Med. Chem. Lett. 23*, 2001−2006.